# Linking dissipation-induced instabilities with nonmodal growth: The case of helical magnetorotational instability

Mamatsashvili, G.; Stefani, F.;

Originally published:

November 2016

**Physical Review E 94(2016)5, 051203(R)**

DOI: https://doi.org/10.1103/PhysRevE.94.051203

# Linking dissipation-induced instabilities with nonmodal growth: the case of helical magnetorotational instability

G. Mamatsashvili[1,2,3*] and F. Stefani[1†]
[1] *Helmholtz-Zentrum Dresden-Rossendorf, P.O. Box 510119, D-01314 Dresden, Germany*
[2] *Department of Physics, Faculty of Exact and Natural Sciences, Tbilisi State University, Tbilisi 0179, Georgia*
[3] *Abastumani Astrophysical Observatory, Ilia State University, Tbilisi 0162, Georgia*
(Dated: October 18, 2016)

The helical magnetorotational instability is known to work for resistive rotational flows with comparably steep negative or extremely steep positive shear. The corresponding lower and upper Liu limits of the shear are continuously connected when some axial electrical current is allowed to flow through the rotating fluid. Using a local approximation we demonstrate that the magnetohydrodynamic behavior of this dissipation-induced instability is intimately connected with the nonmodal growth and the pseudospectrum of the underlying purely hydrodynamic problem.

PACS numbers: 47.32.-y, 47.35.Tv, 47.85.L-, 97.10.Gz, 95.30.Qd

The magnetorotational instability (MRI) [1] is believed to trigger turbulence and transport of angular momentum in magnetized accretion disks [2]. The typical Keplerian rotation of the disks belongs to a wider class of flows with decreasing angular velocity and increasing angular momentum that are Rayleigh-stable [3], but susceptible to the standard version of MRI (SMRI), with a vertical magnetic field $B_z$ imposed on the rotating flow. For SMRI to operate, both the rotation period and the Alfvén crossing time (equal to the ratio of characteristic scale of the system and Alfvén velocity) have to be shorter than the timescale for magnetic diffusion [4]. For a disk of scale height $H$, this implies that both the magnetic Reynolds number $\mathrm{Rm} = \mu_0\sigma H^2\Omega$ and the Lundquist number $S = \mu_0\sigma H v_A$ must be larger than one ($\Omega$ is the angular velocity, $\mu_0$ the magnetic permeability, $\sigma$ the conductivity, $v_A$ the Alfvén velocity).

These conditions are safely fulfilled in well-conducting parts of accretion disks. The situation with SMRI is less clear in the "dead zones" of protoplanetary disks, in stellar interiors, and in the liquid cores of planets, because of low magnetic Prandtl numbers $\mathrm{Pm} = \nu/\eta$ there, i.e., the ratio of viscosity $\nu$ to magnetic diffusivity $\eta = (\mu_0\sigma)^{-1}$ [5, 6]. Moreover, in compact objects, like stars and planets, even the condition of decreasing angular velocity, necessary for SMRI, is not everywhere fulfilled: a counter-example is the equator-near strip of the solar tachocline [7], which is also the region of sunspot activity [8].

The helical version of MRI (HMRI) is interesting both with respect to the low-Pm problem as well as for regions with positive shear. Adding an azimuthal magnetic field $B_\phi$ to $B_z$, Hollerbach and Rüdiger [9] had shown that this dissipation-induced instability works also in the inductionless limit, $\mathrm{Pm} = 0$, and scales with the Reynolds number $\mathrm{Re} = \mathrm{RmPm}^{-1}$ and the Hartmann number $\mathrm{Ha} = S\mathrm{Pm}^{-1/2}$, in contrast to SMRI that is governed by Rm and $S$. Soon after, Liu et al. [10] showed that HMRI is restricted to rotational flows with negative shear slightly steeper than the Keplerian, or extremely steep positive shear. Specifically, their short-wavelength analysis gave a threshold of the negative steepness of the rotation profile $\Omega(r)$, expressed by the Rossby number $\mathrm{Ro} = r(2\Omega)^{-1}\partial\Omega/\partial r$, of $\mathrm{Ro_{LLL}} = 2(1-\sqrt{2}) \approx -0.8284$, and a corresponding threshold of the positive shear, at $\mathrm{Ro_{ULL}} = 2(1+\sqrt{2}) \approx 4.8284$ (LLL and ULL refer to the lower and upper Liu limits, respectively).

Surprisingly, the same Liu limits were later found [11, 12] to apply also to the azimuthal MRI (AMRI) – a non-axisymmetric "sibling" of the axisymmetric HMRI that prevails for large ratios of $B_\phi$ to $B_z$ [13]. Recently, the destabilization of steep positive shear profiles by purely azimuthal fields was demonstrated by means of both a short-wavelength analysis [14] and a one-dimensional stability analysis for a Taylor-Couette flow with narrow gap [15].

By allowing axial electrical currents not only at the axis, but also within the fluid, i.e. by enabling the radial profile $B_\phi(r)$ to deviate from the current-free case $\propto 1/r$, it was recently shown [12] that the LLL and the ULL are just the endpoints of one instability curve in a plane that is spanned by Ro and a corresponding steepness of the azimuthal magnetic field, called magnetic Rossby number, $\mathrm{Rb} = r(2B_\phi/r)^{-1}\partial(B_\phi/r)/\partial r$. In the limit of large Re and Ha, this curve acquires the closed form

$$\mathrm{Rb} = -\frac{1}{8}\frac{(\mathrm{Ro}+2)^2}{\mathrm{Ro}+1}. \qquad (1)$$

A consequence of this curve is the strictness of the lower Liu limit $\mathrm{Ro_{LLL}} = -0.828$, which would prevent Keplerian profiles $\mathrm{Ro_{Kep}} = -0.75$ from being destabilized by HMRI or AMRI, could be relaxed if only a small amount of the axial current is allowed to pass through the liquid. This effect is now to be investigated in a planned liquid sodium Taylor-Couette experiment [16], which will combine and enhance the previous experiments on HMRI [17], AMRI [18] and the kink-type Tayler-instability [19].

Apart from these interesting achievements, the very

existence of the two Liu limits has remained an unexplained conundrum. This paper aims at linking these magnetohydrodynamic features to the nonmodal dynamics of perturbations in the purely hydrodynamic case.

The nonmodal approach to the stability analysis of shear flows focuses on the finite-time dynamics of perturbations, accounting for transient phenomena due to the shear-induced nonnormality of the flow [20–24], in contrast to the canonical modal approach, which is concerned with the behavior at large times. It consists in calculating the optimal initial perturbations with a given positive norm that lead to the maximum possible linear amplification during some finite time. In self-adjoint problems, the perturbations that undergo the largest amplification are essentially the most unstable normal modes. By contrast, in non-selfadjoint shear flow problems, the normal mode eigenfunctions are nonorthogonal due to the nonnormality, resulting in transient, or nonmodal growth of perturbations, which can be substantially higher than that of the most unstable normal mode [22, 25]. So, leaving out the effects of the nonnormality can lead to an incomplete picture of the overall dynamics (stability) of shear flows.

Our main goal is to examine the nonmodal dynamics of HMRI in differentially rotating flows, which represent a special class of shear flows, for which the nonnormality inevitably plays a role. This can result in growth factors over intermediate (dynamical/orbital) times larger than the modal growth of HMRI. Recently, the nonmodal dynamics of SMRI was studied in [25, 26]; the present study extends these investigations to the highly resistive, or low-Pm regime, where only HMRI survives.

We start with the equations of nonideal magnetohydrodynamics for incompressible conductive media,

$$\frac{\partial \mathbf{u}}{\partial t} + \mathbf{u}\cdot\nabla\mathbf{u} = -\frac{1}{\rho}\nabla\left(p + \frac{\mathbf{B}^2}{2\mu_0}\right) + \frac{\mathbf{B}\cdot\nabla\mathbf{B}}{\mu_0\rho} + \nu\nabla^2\mathbf{u}, \quad (2)$$

$$\frac{\partial \mathbf{B}}{\partial t} = \nabla\times(\mathbf{u}\times\mathbf{B}) + \eta\nabla^2\mathbf{B}, \quad (3)$$

$$\nabla\cdot\mathbf{u} = 0, \quad \nabla\cdot\mathbf{B} = 0. \quad (4)$$

where $\rho$ is the constant density, $p$ is the thermal pressure, $\mathbf{u}$ is the velocity and $\mathbf{B}$ is the magnetic field.

An equilibrium flow represents a fluid rotating with angular velocity $\Omega(r)$ and threaded by a magnetic field, which comprises a constant axial component $B_{0z}$ and an azimuthal one $B_{0\phi}$ with arbitrary radial dependence:

$$\mathbf{u}_0 = r\Omega(r)\mathbf{e}_\phi, \qquad \mathbf{B}_0 = B_{0\phi}(r)\mathbf{e}_\phi + B_{0z}\mathbf{e}_z.$$

Consider now small axisymmetric ($\partial/\partial\phi = 0$) perturbations about the equilibrium, $\mathbf{u}' = \mathbf{u} - \mathbf{u}_0$, $p' = p - p_0$, $\mathbf{B}' = \mathbf{B} - \mathbf{B}_0$. Following [10, 12, 27] we adopt a local Wentzel–Kramers–Brillouin (WKB) approximation in the radial direction around some fiducial radius $r$, i.e., we assume perturbation lengthscales much shorter than the characteristic lengths of radial variations of the equilibrium quantities, and represent perturbations as $\mathbf{u}', \mathbf{B}' \propto \exp(\mathrm{i}k_r r + \mathrm{i}k_z z)$, with axial $k_z$ and large radial $k_r$ wavenumbers, $rk_r \gg 1$. Linearizing Eqs. (2)-(4) about the equilibrium and normalizing time by $\Omega^{-1}$, we arrive at the following equations for the perturbations (see [12, 25] for details):

$$\frac{d\boldsymbol{\psi}}{dt} = \mathbf{A}\cdot\boldsymbol{\psi}, \quad (5)$$

where $\boldsymbol{\psi} \equiv (u_r', u_\phi', B_r', B_\phi')$ is the state vector and the evolution matrix operator $\mathbf{A}$, which is independent of time for axisymmetric perturbations, is given by (the factor $(\mu_0\rho)^{-1/2}$ is absorbed in the magnetic field)

$$\mathbf{A} = \begin{pmatrix} -\frac{1}{\mathrm{Re}} & 2\alpha^2 & \mathrm{i}\omega_z & -2\omega_\phi\alpha^2 \\ -2(1+\mathrm{Ro}) & -\frac{1}{\mathrm{Re}} & 2\omega_\phi(1+\mathrm{Rb}) & \mathrm{i}\omega_z \\ \mathrm{i}\omega_z & 0 & -\frac{1}{\mathrm{Rm}} & 0 \\ -2\omega_\phi\mathrm{Rb} & \mathrm{i}\omega_z & 2\mathrm{Ro} & -\frac{1}{\mathrm{Rm}}, \end{pmatrix}$$

with $\alpha = k_z/k$, $k^2 = k_r^2 + k_z^2$, $\omega_z \equiv k_z B_{0z}/\Omega$ and $\omega_\phi \equiv B_{0\phi}/r\Omega$. The Reynolds number, $\mathrm{Re} = \Omega/\nu k^2$, and the magnetic Reynolds number, $\mathrm{Rm} = \Omega/\eta k^2$ are chosen as $\mathrm{Re} = 4000$ and $\mathrm{Rm} = 0.012$, to give a small magnetic Prandtl number $\mathrm{Pm} = \mathrm{Rm}/\mathrm{Re} = 3\cdot 10^{-6}$ typical for liquid metals and protoplanetary disks [5]. The strength of the imposed axial field is measured by the Hartmann number $\mathrm{Ha} = \omega_z\sqrt{\mathrm{Re}\cdot\mathrm{Rm}}$, which is fixed to $\mathrm{Ha} = 15$, close to experiments [17], and the azimuthal field by $\beta = \omega_\phi/\omega_z$. HMRI is most effective for $\beta \sim 1$ [9, 10, 12]. We consider Rayleigh-stable rotation with $\mathrm{Ro} > -1$ and $\mathrm{Rb} < 0$, since the axial current decreases with radius. It is shown that $\mathbf{A}$ is nonnormal (non-selfadjoint), i.e., does not commute with its adjoint, $\mathbf{A}^\dagger\cdot\mathbf{A} \neq \mathbf{A}\cdot\mathbf{A}^\dagger$ and the degree of the nonnormality increases with shear ($|\mathrm{Ro}|$).

We quantify the nonmodal amplification in terms of the total perturbation energy, $E = \frac{\rho}{2}(|\mathbf{u}'|^2 + |\mathbf{B}'|^2) = \boldsymbol{\psi}^\dagger\cdot F^\dagger F\cdot\boldsymbol{\psi}$, where $\mathbf{F} = \sqrt{\rho/2}\cdot diag(\alpha^{-1}, 1, \alpha^{-1}, 1)$, which is a physically relevant norm. The maximum possible, or optimal growth at a specific time $t$ is defined as the ratio $G(t) = \max_{\boldsymbol{\psi}(0)} E(t)/E(0)$, where $E(t)$ is the energy at $t$ and the maximization is done over all initial states $\boldsymbol{\psi}(0)$ with a given initial energy $E(0)$ (e.g., Ref. [22]). The final state at $t$ is found from the initial state at $t = 0$ by solving the linear Eq. (5) and can be formally written as $\boldsymbol{\psi}(t) = \mathbf{K}(t)\cdot\boldsymbol{\psi}(0)$, where $\mathbf{K}(t)$ is the propagator matrix. Then, the maximum possible amplification $G(t)$ is usually calculated by the singular value decomposition of $\mathbf{K}$ at $t$ (e.g., Refs. [21–24]). The square of the largest singular value gives the value of $G(t)$ and the corresponding initial condition that leads to this growth (optimal perturbations) is given by the right singular vector. Note again that the nonmodal approach combined with the method of optimal perturbations is the most general way

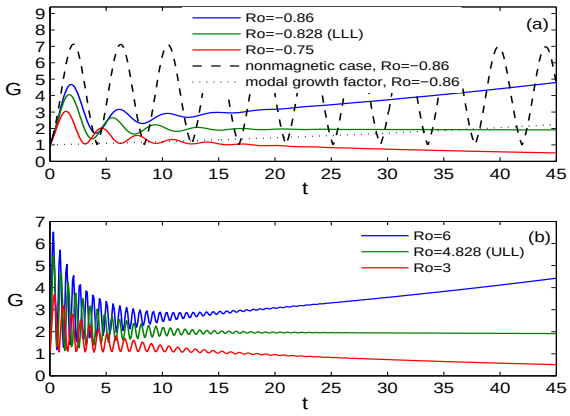


FIG. 1. Maximum growth $G(t)$ vs. $t$ at different (a) Ro $= -0.86, -0.828(\mathrm{LLL}), -0.75(\mathrm{Kepler})$ and (b) Ro $= 3, 4.828(\mathrm{ULL}), 6$. Other parameters are $\alpha = 1, \mathrm{Rb} = -1$. For each pair of Ro and Rb, the parameter $\beta$ is chosen such as to maximize the modal growth rate for given other parameters.

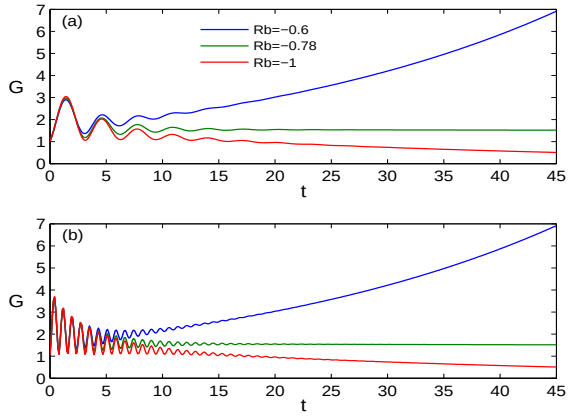


FIG. 2. Maximum growth $G(t)$ vs. $t$ at different Rb $= -1, -0.78, -0.6$ and at fixed (a) $\mathrm{Ro_{Kep}} = -0.75$ and (b) Ro $= 3$ both with $\alpha = 1$.

of analyzing shear flow dynamics at all times, as opposed to the modal approach, which concentrates only on the behavior at asymptotic times and hence omits important finite-time transient phenomena.

The modal analysis in the WKB approximation yields an expression for the growth rate of HMRI in the relevant limit of small Pm $\to 0$ and small interaction parameter (Elsasser number), $\mathrm{Ha}^2/\mathrm{Re} \ll 1$, but large Re $\to \infty$ [10, 12]. When maximized with respect to $\beta$ (which is typically around unity), this growth rate, given by Eq. (8.30) of [12], becomes (in units of $\Omega$)

$$\gamma = -\frac{\mathrm{Ha}^2}{\mathrm{Re}}\left[\frac{(\mathrm{Ro}+2)^2}{8(1+\mathrm{Ro})\mathrm{Rb}} + 1\right], \qquad (6)$$

while the real part of the eigenfrequency is equal to the frequency of inertial waves, $\omega_{\mathrm{iw}} = 2\alpha\sqrt{1+\mathrm{Ro}}$. Equation

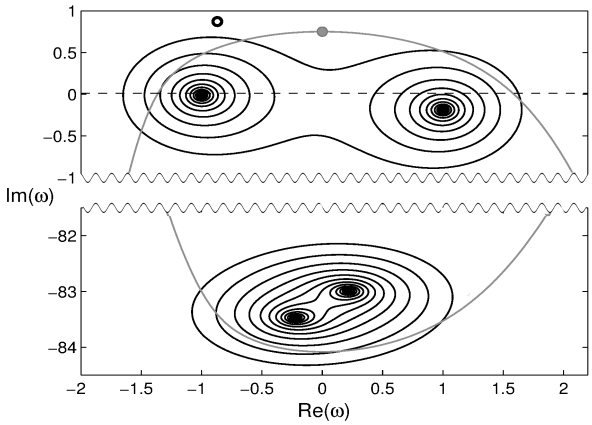


FIG. 3. Isolines at $\epsilon = 10^{0.25}, 10^{0.4}, 10^{0.55}, ..., 10^{3.1}$ show the $\epsilon$-pseudospectra of the $\mathbf{A}$ matrix in the complex $\omega$-plane for $\mathrm{Rb} = -1, \alpha = 1$ and $\mathrm{Ro_{Kep}} = -0.75$. The circle indicates the complex $\omega_K$ corresponding to the Kreiss constant. The gray curve shows numerical range and the dot on it is the numerical abscissa. Four black dots represent the eigenvalues of the normal modes.

(6) yields the stability boundary Eq. (1) which indicates that for Rb $= -1$ the instability (i.e., $\gamma > 0$) exists at negative, Ro $< \mathrm{Ro_{LLL}} = -0.828$, and positive, Ro $> \mathrm{Ro_{ULL}} = 4.828$, shear, while at larger $-1 <$ Rb $< 0$, the stability region shrinks and the instability extends beyond the Liu limits. As a result, the modal growth of HMRI can also exist for the Keplerian rotation ($\mathrm{Ro_{Kep.}} = -0.75$) starting from Rb $= -0.781$ [12].

Now we examine the nonmodal growth of HMRI versus time. Figures 1 and 2 show the maximum energy growth $G(t)$ at modally stable and unstable Ro and Rb together with the growth in the modally stable nonmagnetic case, where only the nonmodal growth is possible. For comparison, the dotted curve in Fig. 1(a) shows the modal growth factor of the energy vs. time, $\exp(2\gamma t)$, for the most unstable normal mode at Ro $= -0.86$ with the corresponding growth rate $\gamma$ given by Eq. (6). In all cases, the initial stage of evolution is qualitatively similar: the energy increases with time, reaches a maximum $G_m$ and then decreases. This first nonmodal amplification phase is followed by minor amplifications. Like in the case of modal growth, the kinetic energy dominates over the magnetic one also during nonmodal growth. As a result, the duration of each amplification event is set by inertial waves: the peak value $G_m$ is attained at around one quarter of the wave period, $t_m \approx \pi/2\omega_{\mathrm{iw}}$, similar to that in the nonmagnetic case, although its value is smaller than that in the latter case. At larger times, the optimal growth follows the behavior of the modal solution – it increases (for Ro $= -0.86, 6$), stays constant (for the Liu limits, Ro $= \mathrm{Ro_{LLL}}, \mathrm{Ro_{ULL}}$) or decays

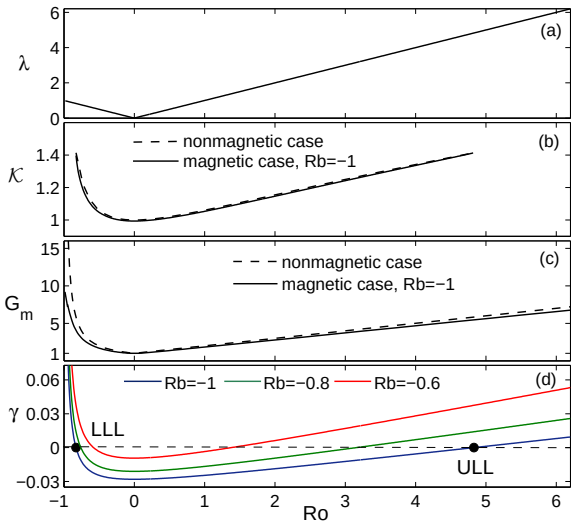


FIG. 4. (a) numerical abscissa, $\lambda$, (b) Kreiss constant, $\mathcal{K}$ (c) $G_m$ for HMRI at Rb $= -1$ as well as in the nonmagnetic case and (d) modal growth rate $\gamma$ of HMRI from Eq. (6) vs. Ro at different Rb $= -1, -0.8, -0.6$ and $\alpha = 1$.

(for Ro $= -0.75, 3$), respectively, if the flow is modally unstable, neutral or stable; in the latter case HMRI undergoes only transient amplification. This is readily understood: at large times the least stable modal solution (with growth rate given by Eq. 6) dominates, whereas at small and intermediate times the transient growth due the interference of nonorthogonal eigenfunctions is important. In particular, for the Liu limits, where the modal growth is absent, there is moderate nonmodal growth $G_m(\mathrm{Ro_{LLL}}) = 4.06, G_m(\mathrm{Ro_{ULL}}) = 5.46$. A similar evolution of axisymmetric perturbations' energy with time for HMRI was already found in [28], where also the physical mechanism of HMRI was explained in terms of an additional coupling between meridional and azimuthal flow perturbations. Importantly, in Fig. 1, $G$ at modally stable and unstable Rossby numbers are comparable and several times larger than the modal growth factors during the same time. Indeed, at Ro $= -0.86$, the nonmodal growth achieves the first peak $G_m = 4.68$ at $t_m = 1.86$, while from the dotted curve in Fig. 1(a), which shows the growth of the most unstable mode at the same Ro, we see that by time $t_m$ energy of the latter would have grown only by a factor of $\exp[2\gamma(\mathrm{Ro})t_m] = 1.034$. This also implies that in the Keplerian regime, where there is no modal growth of HMRI for Rb $= -1$, it still exhibits moderate nonmodal growth (red curves in Figs. 1a and 2a). It is seen from Fig. 2 that $G_m$ is almost insensitive to Rb, but its effect becomes noticeable as time passes. Decreasing the slope at a given Ro increases the optimal growth and at large times renders the flow modally unstable.

The other notions used to characterize the nonmodal growth and its connection with the results of modal analysis are the pseudospectra and numerical range of the nonnormal operator $\mathbf{A}$ [22–24]. The maximal protrusion of the numerical range into the upper (unstable) half in the complex $\omega$-plane – a numerical abscissa, $\lambda$ – defines the maximum growth rate at the beginning of evolution (at $t = 0^+$), $2\lambda = \max_{\boldsymbol{\psi}(0)} E(t)^{-1} dE(t)/dt|_{t=0^+}$. On the other hand, the extent to which the pseudospectra contours penetrate into the upper half of $\omega$-plane determines the amount of transient amplification over time. This is quantified by the Kreiss constant $\mathcal{K} = \max_{\mathrm{Im}(\omega)>0} \mathrm{Im}(\omega)||(\mathbf{A} + \mathrm{i}\omega\mathbf{I})^{-1}||$, where $\mathbf{I}$ is the unit matrix and $||\cdot||$ denotes an appropriately defined norm [22, 23]. It provides a lower estimate for the maximum nonmodal amplification of energy over time, i.e., $\max_{t>0} G(t) \geq \mathcal{K}^2$ [22, 24].

Figure 3 shows the normal mode spectra of Eq. (5) and the associated pseudospectra in $\omega$-plane at $\mathrm{Ro_{Kep}} = -0.75$, where all the eigenfrequencies (black dots) are in the lower half plane, indicating modal stability against HMRI. The mode which is closer to the $\mathrm{Im}(\omega) = 0$-axis will first cross it and exhibit HMRI as Ro changes beyond the Liu limits, while the other two modes far in the lower half plane are rapidly damped magnetic (SMRI) modes. The numerical abscissa and the frequency, $\omega_{\mathcal{K}}$, resulting in the Kreiss constant, lie in the upper plane, which indicates the nonmodal amplification larger than $\mathcal{K}^2$ occurs over intermediate times.

Figure 4, which illustrates our central result, shows (a) the numerical abscissa $\lambda$, (b) the Kreiss constant $\mathcal{K}$, (c) the maximum growth $G_m$ for Rb $= -1$ as well as in the nonmagnetic case and (d) the modal growth rate $\gamma$ given by Eq. (6) at Rb $= -1, -0.8, -0.6$ versus Ro. The numerical abscissa, giving the initial optimal growth rate of the energy, is equal to |Ro|, i.e., to the maximum growth rate of ideal SMRI (see Ref. [25]) despite the high resistivity of the flow. $G_m$ increases linearly with Ro at Ro $> 0$ and much steeper at Ro $< 0$ which can be well approximated by $\propto (1+\mathrm{Ro})^{-0.78}$. For comparison, in this plot we also show the maximum transient growth factor for axisymmetric perturbations in the nonmagnetic case, $G_m^{(h)} = (1 + \mathrm{Ro})^{\mathrm{sgn(Ro)}}$, from [29]. So, although $G_m$ in the magnetic case is slightly smaller than that in the nonmagnetic one, the two curves are in fact close to each other and display nearly the same behavior with Ro, a feature that is also shared by the Kreiss constant (b). Note that the dependencies of $G_m$, $G_m^{(h)}$ (Fig. 4c) and of the modal growth rate $\gamma$ (Fig. 4d) on Ro have very similar shapes. Remarkably, the latter, being given by Eq. (6), can be expressed in terms of the hydrodynamic nonmodal growth $G_m^{(h)} = (1 + \mathrm{Ro})^{\mathrm{sgn(Ro)}}$ in the closed form (for Rb $= -1$)

$$\gamma = \frac{\mathrm{Ha}^2}{\mathrm{Re}} \left[ \frac{(G_m^{(h)} + 1)^2}{8 G_m^{(h)}} - 1 \right] \qquad (7)$$

which is indeed proportional to $G_m^{(h)}$ for larger values.

Both Liu limits are therefore connected with a corresponding threshold $G_m^{(h)}(\mathrm{Ro}_{\mathrm{LLL}}) = G_m^{(h)}(\mathrm{Ro}_{\mathrm{ULL}}) = 5.828$.

In this paper, we have investigated the nonmodal dynamics of HMRI due to the nonnormality of a magnetized shear flow with large resistivity. The nonmodal growth of HMRI is generally several times larger than its modal growth during the dynamical time. Notably, in the case of current-free azimuthal field, the moderate nonmodal growth also occurs in the Keplerian regime, where the modal HMRI is non-existent (Fig. 1). As illustrated in Fig. 4 and quantified exactly in Eq. (7), the modal growth rate of HMRI displays a very similar dependence on Ro as the maximum nonmodal growth in the purely hydrodynamic shear flow, which indicates a fundamental connection between nonmodal dynamics and dissipation-induced modal instabilities, such as HMRI. Both, despite the latter being magnetically triggered, rely on hydrodynamic means of amplification, i.e., extract energy from the background flow mainly by Reynolds stress due to shear/nonormality [28].

Because of the general character of linear Eq. (5) the results obtained here can, in principle, apply to any differentially rotating magnetized cylindrical flow system with viscosity and resistivity threaded by helical magnetic field. Such systems are ubiquitous, ranging from laboratory [17, 18] to liquid cores of planets, stars and protoplanetary disks. It is the differential rotation (shear) that plays a pivotal role, and all these objects involve this type of nonuniform motion to various extent. MRI was already examined in the resistive liquid core of the Earth [6] and in stars [7, 30–32] by means of the modal approach, thereby missing out nonmodal effects.

The next step will be to generalize the nonmodal analysis to AMRI, which consists in the growth of non-axisymmetric perturbations. Recently, it was shown in [33] that in a hydrodynamic Taylor-Couette flow the effects of nonnormality play an important role, resulting in large ($\sim Re^{2/3}$) transient amplification of non-axisymmetric modes. Since the amplification in the highly resistive regime is determined by velocity shear, it is expected that the nonnormality will influence AMRI too, although the dynamics is more complex compared to that for axisymmetric HMRI due to the time-dependence of the radial wavenumber.

This work is supported by Alexander von Humboldt Foundation and German Helmholtz Association in frame of Helmholtz Alliance LIMTECH.

* g.mamatsashvili@hzdr.de
† f.stefani@hzdr.de

[1] E.P. Velikhov, JETP **9**, 995 (1959).
[2] S.A. Balbus, J.F. Hawley, Rev. Mod. Phys. **70**, 1 (1998).
[3] Lord Rayleigh, Proc. R. Soc. London A **93**, 148 (1917).
[4] W. Liu, J. Goodman, H. Ji, Astrophys. J. **643**, 306 (2006)
[5] S.A. Balbus, P. Henri, Astrophys. J. **674**, 408 (2008)
[6] L. Petitdemange, E. Dormy, S. Balbus, Geophys. Res. Lett., **35**, L15305 (2008)
[7] K.P. Parfrey, K. Menou, Astrophys. J. Lett. **667**, L207 (2007)
[8] P. Charbonneau, Liv. Rev. Sol. Phys. **7**, 3 (2010)
[9] R. Hollerbach, G. Rüdiger, Phys. Rev. Lett. **95**, 124501 (2005)
[10] W. Liu, J. Goodman, I. Herron, H. Ji, Phys. Rev. E **74**, 056302 (2006)
[11] O. Kirillov, F. Stefani, Astrophys. J., **712**, 52 (2010); O.N. Kirillov, F. Stefani, Y. Fukumoto, Astrophys. J. **756**, 83 (2012); O. Kirillov, F. Stefani, Phys. Rev. Lett. **111**, 061103 (2013)
[12] O. Kirillov, F. Stefani, Y. Fukumoto, J. Fluid Mech. **760**, 591 (2014)
[13] R. Hollerbach, V. Teeluck, G. Rüdiger, Phys. Rev. Lett. **104**, 044502 (2010)
[14] F. Stefani, O. Kirillov, Phys. Rev E **92**, 051001(R) (2015)
[15] G. Rüdiger et al. Phys. Fluids **28**, 014105 (2016).
[16] F. Stefani et al., Magnetohydrodynamics, **4**8, 103 (2012)
[17] F. Stefani et al., Phys. Rev. Lett. **97**, 184502 (2006); F. Stefani et al., Phys. Rev. E. **80**, 066303 (2009)
[18] M. Seilmayer et al., Phys. Rev. Lett. **113**, 024505 (2014)
[19] M. Seilmayer et al., Phys. Rev. Lett. **108**, 244501 (2012)
[20] L. Trefethen, A. Trefethen, S. Reddy, T. Driscoll, Science, **261**, 578 (1993)
[21] B. Farrell, P. Ioannou, J. Atmos. Sci. **53**, 2025 (1996)
[22] P. Schmid, D. Henningson, Stability and Transition in Shear Flows (Springer Verlag, New York, 2001)
[23] L. Trefethen, M. Embree, Spectra and Pseudospectra, The behavior of Nonnormal Matrices and Operators (Princeton University Press, Princeton, NJ, 2005)
[24] P. Schmid, Annu. Rev. Fluid Mech., **39**, 129 (2007)
[25] J. Squire, A. Bhattacharjee, Phys. Rev. Lett., **113**, 025006 (2014); J. Squire, A. Bhattacharjee, Astrophys. J., **797**, 67 (2014)
[26] G. Mamatsashvili, G. Chagelishvili, G. Bodo, P. Rossi, Mon. Not. R. Astron. Soc., **435**, 2552 (2013)
[27] M. Pessah, D. Psaltis, Astrophys. J., **628**, 879 (2005)
[28] J. Priede, I. Grants, G. Gerbeth, Phys. Rev. E, **75**, 047303 (2007)
[29] N. Afshordi, P. Mukhopadhyay, R. Narayan, Astrophys. J., **629**, 373 (2005)
[30] R. Arlt, R. Hollerbach, G. Rüdiger, Astron. Astrophys., **401**, 1087 (2003)
[31] D. Kagan, J. C. Wheeler, Astrophys. J., **787**, 20 (2014)
[32] L. Jouve, T. Gastine, F. Ligniéres, Astron. Astrophys., **575**, 18 (2015)
[33] S. Maretzke, B. Hof, M. Avila, J. Fluid Mech., **742**, 254 (2014)